Rain retrieval method for mesoscale convective systems

M. P. CADEDDU [1], C. PRABHAKARA [2], G. DALU [1](*) and R. IACOVAZZI [3]

[1] *Area della Ricerca del CNR - Via Bottego 7, 09125 Cagliari, Italy*
[2] *Goddard Space Flight Center, NASA - Greenbelt, MD 20771, USA*
[3] *Hughs, STX - Lanham, MD 20081, USA*

(ricevuto il 26 Novembre 1997; revisionato il 10 Dicembre 1998; approvato il 29 Gennaio 1999)

Summary. — The analysis of recent high-resolution aircraft observations over the ocean made by radar and passive microwave radiometer reveals significant problems in relating the brightness temperature measurements of the radiometer with the radar-derived rain rates. A predominant cause of this problem is that the information on rain drops contained in the radiometric measurements is contaminated by scattering and emission from other hydrometeors present in the field of view (fov) of the radiometer. Extensive observations of rain rate made by ship-borne radars and by the multichannel Special Sensor Microwave Imager (SSM/I), with a much larger fov, lead to similar conclusions. Considering the variability in the meteorological conditions, and in the hydrometeors spatial distribution, we developed an empirical method to estimate rain rate based on two parameters derived from the SSM/I data, which are related to the convective dynamics. The calibration of this empirical algorithm was performed with radar ground truth for November 1992, available over the TOGA-COARE (Tropical Ocean Global Atmosphere-Coupled Ocean Atmosphere Response Experiment) region. Then the algorithm was applied to the same TOGA-COARE region for the remaining three months available. The comparison between the estimated rain rate and the radar observations gives a correlation coefficient of about 0.85, and the monthly total estimated rainfall has an error of about 13%. This rain retrieval method, tuned for Mesoscale Convective Systems (MCSs), is applicable to the Tropical Rain Measuring Mission (TRMM), where microwave radiometric observations and simultaneous radar observations are available.

PACS 92.60 – Meteorology.

1. – Introduction

Joint aircraft observations of multichannel microwave radiometer and radar made by Heymsfield *et al.* (1996) over the Atlantic ocean adjacent to Florida, reveal

(*) E-mail: g.dalu@area.ca.cnr.it

significant problems in relating the brightness temperatures measured by the microwave radiometer with the radar-derived rain rate on a scale of a few kilometers. Also, the analysis of these aircraft observations shows that the information on rain rates contained in the Special Sensor Microwave Imager (SSM/I) brightness temperature data is weak, and that it is significantly contaminated by emission from other hydrometeors present in the clouds (see also McGhaughey and Zipser, 1996).

Rain retrieval algorithms were evaluated by the Algorithm Intercomparison Project (AIP) (Ebert, 1996) utilizing the ship-borne radar observations over the TOGA-COARE area. In that intercomparison, theoretical and empirical algorithms were evaluated for several rain events, and they explained only about 50% of the variance contained in the instantaneous rain rates on a scale of about 15 to 30 km. Furthermore, the retrieved mean rain rates, averaged over a time period of about 30 days (time span of a ship cruise in the TOGA-COARE) and over an area of about 300×300 km^2 (radar-scan area), showed errors of about 50% when compared to radar data. The average rain rate was systematically underestimated by about 50% in the first cruise and overestimated by about 50% in the following cruise, about one month later. These systematic biases are linked to variations in meteorological conditions on a time scale of a month to a season.

Radar rain retrieval methods are much more efficient in sensing rain drops, since the backscatter of microwave varies as $\mathbf{d}^6$, where $\mathbf{d}$ is the diameter of the rain drops (Battan, 1973). On the contrary, in the passive microwave radiometer rain retrieval techniques, the effect of the physical processes of emission and/or scattering by hydrometeors present in a vertical column of the atmosphere varies approximately as $\mathbf{d}^3$ (Olson *et al.*, 1996).

Since microwave brightness temperature measurements do not contain sufficient information to retrieve rain rate in different meteorological conditions, on a spatial scale of about 30 km, we have developed an empirical rain estimation method that includes implicitly some information about the MCS dynamics.

Studies of Doneaud *et al.* (1984) and Lopez *et al.* (1989) based on radar observations show evidence of the importance of the rain area and its relationship to area-average rain rate. The GOES Precipitation Index (GPI) method of Arkin and Meisner (1987) based on satellite infrared radiometric data also depends on the rain area as a principal parameter. Based on these studies, we have introduced the rain area in the microwave-radiometer rain retrieval method. This parameter emphasizes the importance of macroscopic structure that relates more closely to MCS dynamics in the atmosphere, rather than the microscopic properties of the rain.

2. – The rain retrieval method

Radar observations over the TOGA-COARE region in the equatorial Pacific reveal several useful properties of the maritime tropical rain (Short *et al.*, 1997). Since these radars operated continuously, we could follow the life cycle of the MCSs in this region that lasted for several hours. In the early stages of the MCSs, rain from convective cells that have a scale of 1 to 2 km dominates, and the average convective rainfall is greater than the average stratiform rainfall. Later, stratiform rainfall prevails and radar data show an enhancement of reflectivity around 4.5 km altitude, due to melting snow particles (Meneghini and Kumagai, 1994) that fall slowly inside the stratiform clouds. The spatial distribution of rain at any time during the life cycle of the MCS

follows a probability distribution that is analogous to the log-normal type (Jones and Sims, 1978). Meteorological conditions, such as the vertical distribution of winds, humidity, and temperature, play an important role in determining the intensity of rain, and growth and distribution of various hydrometeors in the convective and stratiform cloud systems (Takahashi *et al.*, 1995; McGaughey and Zipser, 1996; Houze and Betts, 1981).

We find that the information given by the SSM/I measured brightness temperatures $T_{85\,\mathrm{v}}$ and $T_{85\,\mathrm{h}}$ (the vertical and horizontal polarization in the 85 GHz channel) is preferable to other channels. In these channels, atmospheric water vapor, molecular oxygen, and cloud liquid drops have appreciable absorption. Because of this, when there are non-raining clouds with appreciable optical thickness, the brightness temperature in these channels is close to the temperature of the uppermost cloud liquid layers. When rain develops with no ice phase in the cloud, there is a weak scattering of the 85 HGz radiation due to rain drops. However, when ice particles are present in the clouds above the freezing level, they lead to a significant drop in the 85 HGz brightness temperature due to scattering. This temperature depression gives an indirect indication of precipitation below the clouds (Wu and Weinman, 1984; Spencer, 1986; Adler *et al.*, 1991). In addition, the field of view (fov) of the 85 HGz channel, which is about 15 km, is the smallest of all the SSM/I channels.

Based on an examination of the SSM/I data, taken from a satellite orbit over the TOGA-COARE region, we can infer the presence of scattering in a 85 HGz pixel inside this region, and we define a scattering depression $\mathbf{D}_\mathrm{s}$ as

$$\mathbf{D}_\mathrm{s} = (T^0_{85\,\mathrm{h}} - T_{85\,\mathrm{h}}) - \mathbf{C}^0 \,, \tag{1}$$

where $T_{85\,\mathrm{h}}$ is the 85 GHz brightness temperature in the horizontal polarization, $\mathbf{C}^0$ is a constant chosen to set a threshold on $\mathbf{D}_\mathrm{s}$, and

$$T^0_{85\,\mathrm{h}} = T_{85\,P\,\mathrm{max}} - (\mathrm{d}T_{85\,\mathrm{h}}/\mathrm{d}P_{85})\cdot(P_{85\,\mathrm{max}} - P_{85})\,. \tag{2}$$

Here P_{85} is the 85 GHz polarization difference $(T_{85\,\mathrm{v}} - T_{85\,\mathrm{h}})$ at a pixel inside the TOGA-COARE region and $P_{85\,\mathrm{max}}$ is the maximum value at some point A within this region, which has a corresponding value $T_{85\,P\,\mathrm{max}}$ of the brightness temperature. A second point B is chosen at the maximum value $T_{85\,\mathrm{h}\,\mathrm{max}}$ of the brightness temperature in the same region, which has a corresponding value $P_{85\,T\,\mathrm{max}}$ of the polarization difference.

The slope of the line AB, introduced in eq. (2), is

$$(\mathrm{d}T_{85\,\mathrm{h}}/\mathrm{d}P_{85}) = (T_{85\,\mathrm{h}\,\mathrm{max}} - T_{85\,P\,\mathrm{max}})/(P_{85\,T\,\mathrm{max}} - P_{85\,\mathrm{max}})\,, \tag{3}$$

and $T^0_{85\,\mathrm{h}}$ is the largest possible value of $T_{85\,\mathrm{h}}$ in the TOGA-COARE region for any given value of P_{85} (see fig. 1). We assume that $T^0_{85\,\mathrm{h}}$ represents non-raining cloud conditions, and that rain starts when $(T^0_{85\,\mathrm{h}} - T_{85\,\mathrm{h}})$ is greater than the threshold value $\mathbf{C}°$, which is empirically set equal to 6 K. If N is the total number of pixels that fit in the TOGA-COARE region, and n is the number of rain pixels where $\mathbf{D}_\mathrm{s}$ is greater than zero, *i.e.* where rain is present, then the ratio n/N gives the fractional rain area f_R, which is the main parameter in our rain retrieval algorithm, in the TOGA-COARE region:

$$f_\mathrm{R} = n/N \,. \tag{4}$$

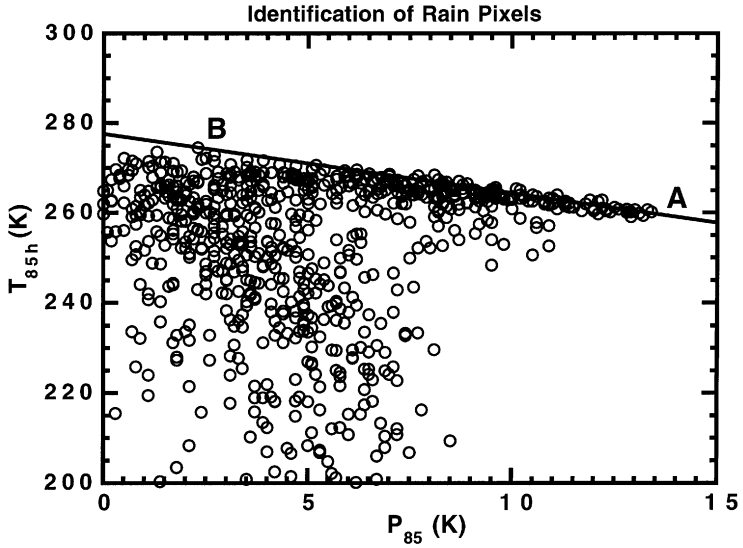

Fig. 1. – Scatter plot of P_{85} *vs.* $T_{85\,\mathrm{h}}$ for the rain event at 10:31 UTC of day 359 (Dec. 24, 1992) observed by F10 SSM/I over the TOGA- COARE region. The line AB gives the largest value of $T_{85\,\mathrm{h}}$ for any given value of P_{85}.

The scattering depression $\mathbf{D}_s$ of eq. (1) is essentially related to an effective optical depth of the ice hydrometeors contained in the layers of the precipitating clouds above the freezing level. We define the scattering index **S** over the entire TOGA-COARE region as

$$\mathbf{S} = (1/N) \sum_{i=1}^{n} \mathbf{D}_{s_i} , \tag{5}$$

where the summation is taken only over those n pixels for which $\mathbf{D}_{s_i}$ is greater than zero, so that the scattering index **S** depends directly on the fractional rain area.

The brightness temperatures at the low frequencies 19 and 37 GHz are strongly related to the emission of hydrometeors (Wilheit *et al.*, 1991; Prabhakara *et al.*, 1992; Petty and Katsaros, 1992; Kummerow *et al.*, 1989), and an emission index **E** in the TOGA-COARE region can be obtained from the same SSM/I data. Let us define P_{19} and P_{37} at a given point in the TOGA-COARE region as $P_{19} = (T_{19\,\mathrm{v}} - T_{19\,\mathrm{h}})$ and $P_{37} = (T_{37\,\mathrm{v}} - T_{37\,\mathrm{h}})$, where $T_{19\,\mathrm{v}}$, $T_{19\,\mathrm{h}}$, $T_{37\,\mathrm{v}}$, and $T_{37\,\mathrm{h}}$ represent the vertical and horizontal polarization brightness temperatures in the 19 and 37 GHz channels, respectively. To a first approximation the quantities P_{19} and P_{37} can be related to the optical depths of the hydrometeors at 19 and 37 GHz.

It can be assumed that where the atmosphere is cloud free, these optical depths represent the relatively small opacities caused by water vapor. At that point P_{19} and P_{37} are determined primarily by the polarizing effect of the sea surface, while at all other points in the TOGA-COARE region the optical depths include the opacity due to cloud liquid drops, rain, and melting and frozen particles in the fov of the radiometer. We can now define an effective emission ratio **e** as

$$\mathbf{e} = P_{19}/P_{37} . \tag{6}$$

This parameter is nearly independent of wind-induced emissivity changes at the surface, and depends essentially on the total content of rain and other hydrometeors in a column of the atmosphere.

By summing **e** taken from the radiometric data in the same n pixels where D_{s_i} is greater than zero, we obtain the total emission due to hydrometeors associated with precipitation present in the grid box. The emission index **E** of the grid box is then defined as

$$\mathbf{E} = (1/N) \sum_{i=1}^{n} \mathbf{e}_i \,. \tag{7}$$

This summation is taken only over the n pixels so that **E**, like **S**, depends directly on the fractional rain area f_R. Although **S** and **E** will be correlated because of this, the ratio **S**/**E** is sufficiently independent of f_R and can be used as a second parameter in the rain retrieval scheme, as shown in fig. 2, obtained from the 87 mesoscale rain events of the four-months TOGA-COARE data. The ratio **S**/**E** adopted is approximately related to the ratio of the optical depth of the ice hydrometeors in the layers of the clouds above the freezing level and the optical depth of the liquid hydrometeors that are below the freezing level. When heavy convective rain is present, this ratio tends to be large because of strong scattering due to frozen dense hydrometeors. For stratiform clouds with less dense ice hydrometeors that scatter weakly, this ratio is relatively small. Moreover, the data in fig. 2 show that there are more cases of heavy convective rain when f_R is small.

Radar rain observations over the same N pixels of the overlap area can be averaged to give the area average rain rate R_A in the TOGA-COARE region, used as ground

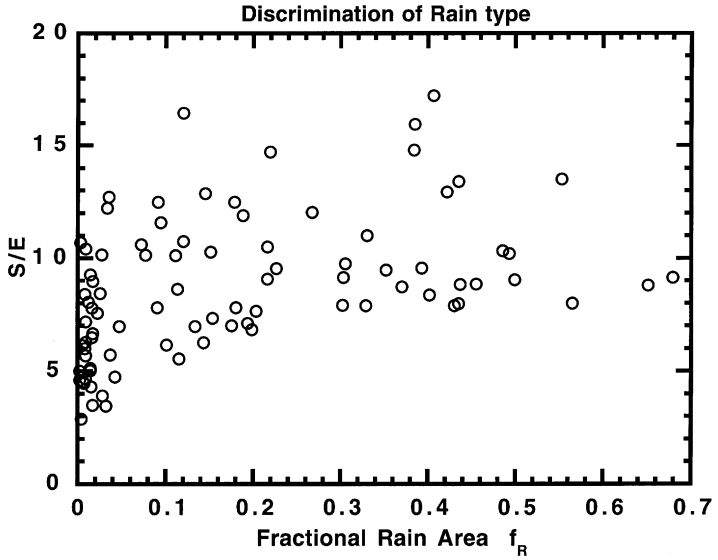

Fig. 2. – Scatter plot of the fractional rain area f_R *vs.* the parameter **S**/**E**, that discriminates convective rain from stratiform rain.

truth for the retrieval method:

$$R_A = (1/N) \sum_{i=1}^{N} R_i \,, \tag{8}$$

where R_i is the radar-derived rain rate in each 85 HGz pixel, that is greater than a fixed threshold of 0.2 mm/h (see the following section).

3. – Rain retrieval over the TOGA-COARE region

From each orbital pass made by the F10 and F11 satellites over the TOGA-COARE region, we can get one combined radar and radiometric data set in the overlap area. We can then choose for our analysis the data sets that contain rain.

It should be pointed out that, in the TOGA-COARE experiment, the radar and radiometric data are not synchronized perfectly in time because the satellite-borne radiometer takes about 50 s to cover 300 km, while the volume scans of the radars take about 10 minutes. For this reason, the fractional rain area f_R determined from radiometric data and the rain rate R_A based on radar data will not be matched perfectly in time (Dalu *et al.*, 1998). In the present study we are dealing with area-time averages, and we can assume that this discrepancy can be neglected. Note that in the Tropical Rain Measuring Mission (TRMM), this discrepancy will be minimized.

To test how well f_R represents the fractional rain area, we have taken a radar-derived rain rate of 0.2 mm/h as a threshold, and we have calculated an alternate fractional rain area $f_{R>0.2}$ in the overlap area. The correlation coefficient between f_R, based on radiometric data, and $f_{R>0.2}$, based on radar data, is about 0.92 for the entire TOGA-COARE data, and we can assume that f_R represents the fractional rain area.

We obtain similar high correlation coefficients between f_R and $f_{R>0.2}$ with values of the threshold $\mathbf{C}^0$ in the range of 3 to 6 K. However, the correlation coefficient decreases significantly with a further increase in $\mathbf{C}^0$, or with an increase in the radar rain-rate threshold.

The area-average rain-rate estimation method developed in this study is based mainly on the four months of TOGA-COARE radar and radiometric observations, with 87 MCS events at different stages of their evolution. In order to assess the relative importance of f_R and $\mathbf{S}/\mathbf{E}$, we have made plots of radar-derived rain rate R_A *vs.* radiometer-derived f_R, and of R_A *vs.* $\mathbf{S}/\mathbf{E}$ as shown in fig. 3a and b. We find that f_R, can explain about 65% of the variance contained in R_A. Furthermore, an examination of fig. 3a reveals that R_A tends to increase non-linearly with respect to f_R. This non-linearity may be approximated with an exponential relationship of the form $R_A = [\exp[kf_R] - 1]$, where k is a constant. The parameter $\mathbf{S}/\mathbf{E}$, on the other hand, can explain only about 25% of the variance contained in R_A.

The indication that R_A grows exponentially with f_R suggests a feedback mechanism. Basically it implies that, as the area of the MCS increases due to intensification of moist dynamics, the area-average rain rate increases in an exponential fashion. Chiu (1988) indicates a similar relationship between fractional rain area and area-average rain rate. We will use this observational information in our rain retrieval method.

We have analyzed the relationship between R_A and f_R on a monthly basis for the entire TOGA-COARE data, and we find that the slope of the regression line between R_A and $[\exp[kf_R] - 1]$ changes considerably from one month to the other. This variation in the slope of the regression line between R_A and $[\exp[kf_R] - 1]$ may be

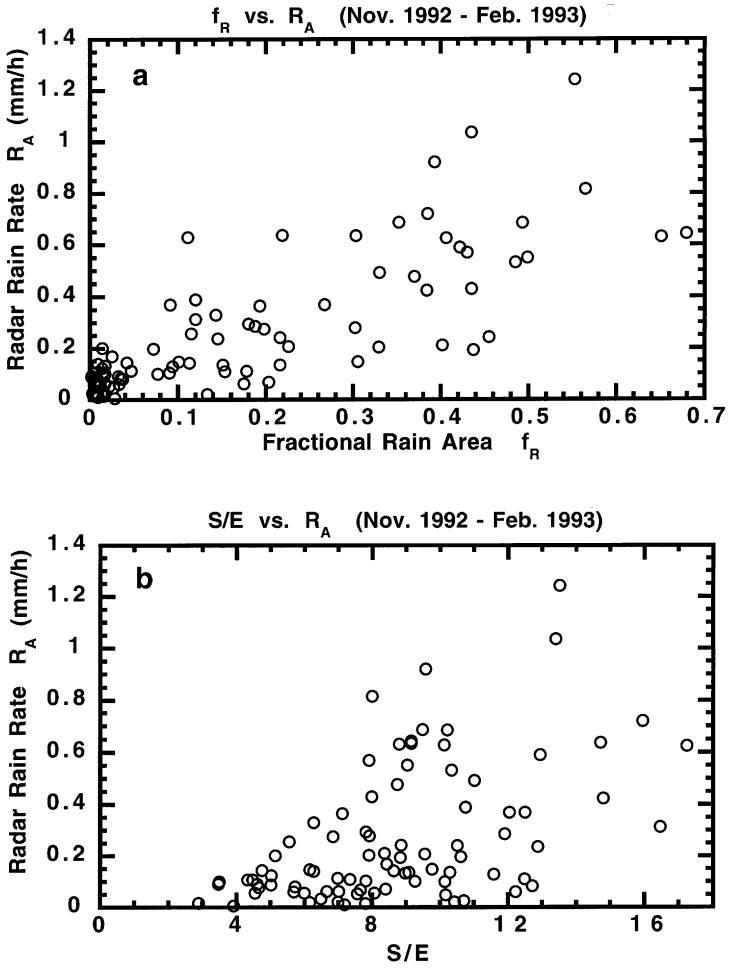

Fig. 3. – a) Scatter plot of fractional rain area f_R *vs.* R_A, the radar-observed rain rate for the four months of the TOGA-COARE observations. b) Scatter plot of the ratio **S/E** *vs.* R_A, for the same data.

related to the changes in the dynamics of the atmosphere, which effect the fractional rain area on a monthly-to-seasonal time scale. So we cannot apply the relationship between R_A and f_R developed from one month of data to estimate the rain rate in another month. However, this is possible by scaling f_R with $(f_{R_{av}})^{0.5}$, where $f_{R_{av}}$ is the monthly mean value of the fractional rain area. From the TOGA-COARE data we find that the slope of the regression line between R_A and $\{\exp[k \cdot f_R/(f_{R_{av}})^{0.5}] - 1\}$ differs, from one month to the other during the TOGA period, only by about 10%. A value of $f_{R_{av}}$ was calculated for the averaging period of one full month, to have a sufficient number of MCS events. This was done for each month of the TOGA-COARE period (November 1992 to February 1993), and the values of $f_{R_{av}}$ derived from the SSM/I data show a significant change from one month to the other. These monthly variations in $f_{R_{av}}$ are consistent with the radar observations.

Based on the exponential dependence of R_A on f_R and the scaling indicated above, the following relationship, that includes the variable $\mathbf{S/E}$, is developed to give the estimated rain rate R_{est} for each month:

$$R_{est} = \exp\left[0.05 \cdot (\mathbf{S/E}) \cdot [f_R / (f_{R_{av}})^{0.5}]\right] - 1 \,. \tag{9}$$

The coefficient 0.05 was obtained by matching R_{est} with the radar ground truth data R_A for the rain events of the month of November 1992, and it is adopted for the independent data sets of the other months. The correlation coefficients between the radar rain rate and the rain rate estimated with eq. (9) for all the rain events in each month are shown in the scatter plots presented in figs. 4a, b, c, and d.

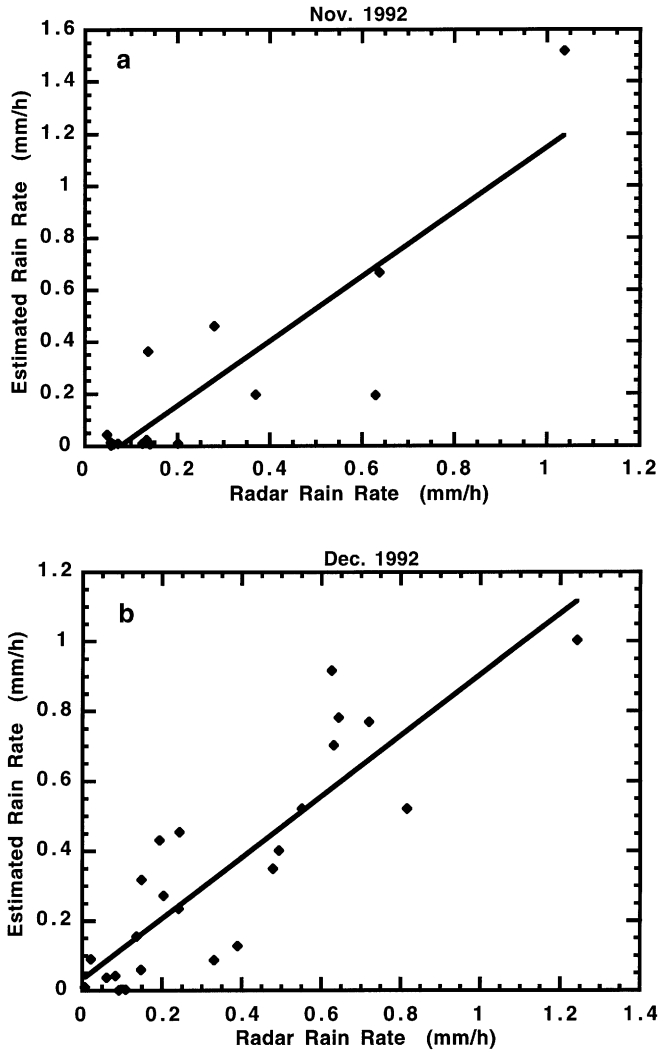

Fig. 4. – Scatter plot of radar observed rain rate R_A *vs.* SSM/I estimated rainfall rate R_{est}. The line indicates the linear regression fit. a) Nov. 1992, Corr. Coeff. = 0.89; b) Dec. 1992, Corr. Coeff. = 0.84.

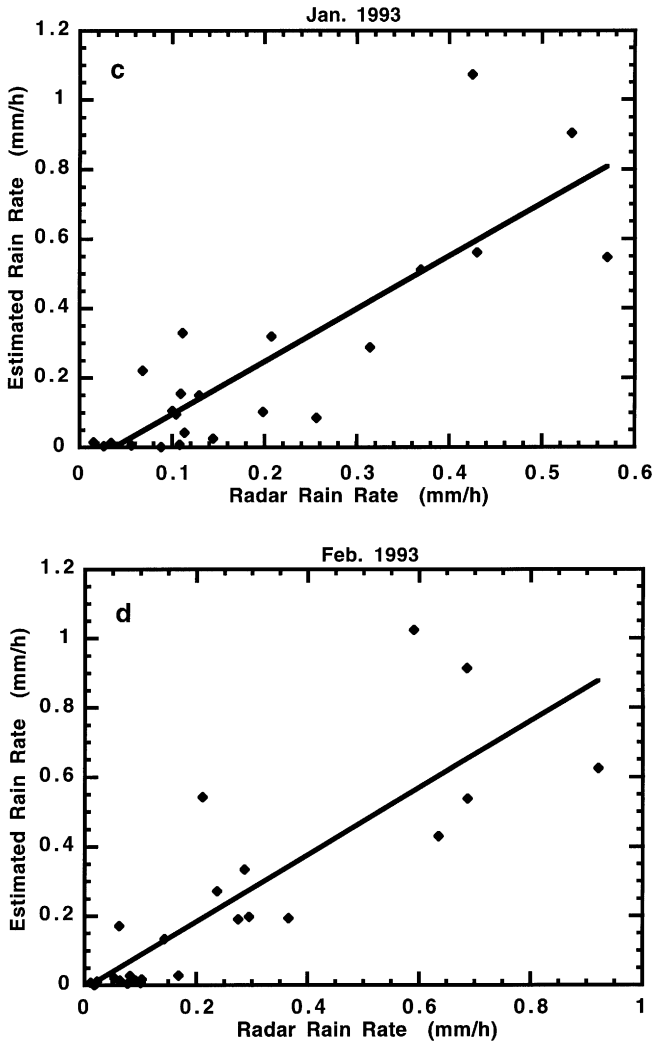

Fig. 4. – Scatter plot of radar observed rain rate R_A *vs.* SSM/I estimated rainfall rate R_{est}. The line indicates the linear regression fit. c) Jan. 1993, Corr. Coeff. = 0.76; d) Feb. 1993, Corr. Coeff. = 0.81.

Since R_{est} given by eq. (9) depends strongly on f_R, this estimate can be more closely related to the dynamics of the atmosphere, rather than to the radiative transfer interactions.

The mean rain rates obtained from all the AIP-3 SSM/I algorithms for each of the three ship cruises (each cruise lasted for about 30 days) were compared with radar data by Ebert (1996). We have done a similar comparison with our retrieval method, and the results are presented in table II below for the three ship cruises within the overlap area in the TOGA-COARE region. The values of f_R are based on the data calculated for each cruise. We note that the percentage error in the retrieved mean rain rate is about 10%. In the retrieval algorithms evaluated by the AIP-3 (Ebert *et al.*, 1996), it was

shown that this percentage error is about 50%, because of the presence of biases. In fact, an underestimation of about 50% in the average rain rate retrieved by the AIP-3 algorithms was found in cruise 1 (11 November 1992 to 10 December 1992), while in cruise 2 (15 December 1992 to 18 January 1993) there was an overestimation of about 50% (see Ebert *et al.*, 1996).

The monthly mean rain rates, shown in table I for the calendar months and in table II for the individual cruises, depend on the scaling parameter $(f_{R_{av}})^{0.5}$ that empirically takes into account month-to-month changes in the dynamical state of the atmosphere. We see that this parameter can change by almost a factor of two in the months considered and it is mainly responsible for the reduction of large errors on a monthly time scale that were found in other algorithms. Furthermore, the instantaneous rain rates retrieved from our algorithm (see figs. 4a, b, c, and d) have a correlation coefficient of about 0.85 with respect to radar observations.

The retrieval method developed here is potentially capable of satisfying the main objective of the TRMM mission, which is to derive monthly-mean rainfall over a latitude-longitude grid box of $5° \times 5°$ with an error of about 10% (Simpson, 1988).

Equation (9) has to be determined with the help of the radar data over a latitude-longitude grid of $5° \times 5°$ and on a time scale of about a month. Since in the TRMM mission about one third of the radiometric data are co-located with the radar data, f_R and the coefficient in eq. (9) can be determined on a month-to-month basis. Since the microwave radiometer and radar will be closely synchronized in the TRMM mission, errors arising from non-simultaneous data should be negligible.

TABLE I. – *Comparison of mean mesoscale rain rates* (mm/h) *within the overlap area for all the* MCS *events in a month.* R_{est} *is estimated from* SSM/I *and* R_A *is observed by radar.* NR *is the number of* MCS *events and* $(f_{R_{av}})$ *is the mean fractional rain area.* $\%\text{Error} = 100 \cdot (R_{est} - R_A)/R_A$.

	NR	Corr. Coeff.	$1/(f_{R_{av}})^{0.5}$	R_A	R_{est}	%Error
Nov. 92	15	0.89	3.17	0.265	0.236	− 11
Dec. 92	24	0.84	1.86	0.358	0.346	− 4
Jan. 93	23	0.76	2.57	0.195	0.242	24
Feb. 93	25	0.81	2.58	0.248	0.229	− 8

TABLE II. – *Same as Table* I, *but for three* TOGA-COARE *ship cruises.* $\%\text{Error} = 100 \cdot (R_{est} - R_A)/R_A$.

	NR	Corr. Coef.	$1/(f_{R_{av}})^{0.5}$	R_A	R_{est}	%Error
Cruise 1 Nov. 10-Dec. 92	20	0.87	3.31	0.235	0.214	10
Cruise 2 Dec. 92-18 Jan. 93	35	0.84	2.04	0.297	0.326	− 9
Cruise 3 Jan. 23-Feb. 93	32	0.82	2.43	0.255	0.236	8

4. – Conclusions

Independent studies (Heymsfield, 1996; McGhaughey and Zipser, 1996; Ebert, 1996) show that the measurements made by multichannel dual-polarization microwave radiometers do not contain sufficient information to retrieve accurate rain rates on a scale comparable to the radiometer field of view. This is mainly because the passive microwave radiometric data have poor sensitivity to rain drops and are contaminated by scattering and emission from other hydrometeors (Smith and Mugnai, 1992). These limitations led us to attempt to retrieve rain rate from microwave radiometric data with an empirical method on a larger scale, such as the scale of MCS events.

We have developed an algorithm that can give mesoscale rain rate over ocean with a correlation coefficient of about 0.85 with respect to the radar data, and also a quantitative estimate of the monthly rainfall. In this method, variation in the rain area produced by the variations in the atmospheric dynamics on a time scale of about a month is factored out in an empirical fashion. This helps to minimize any systematic bias in the estimated monthly-mean rain rate. It is necessary to tune this retrieval method on a monthly basis with the help of the radar data. Backscatter measurements made by a radar operating in the centimeter wavelength range, are more specific to rain drops.

The radiometer rain retrieval method presented here can be used for the TRMM data. In the TRMM mission, satellite-borne radar observations are limited to a narrow swath of 220 km, while the microwave radiometer swath is 760 km wide (Simpson *et al.*, 1996). The radar data overlap with about 30% of the area covered by the radiometer, and this can be used to tune the microwave radiometer rain retrieval method, geographically and seasonally. The radiometer rain retrievals can be used to fill gaps, in space and time, in the radar data and improve spatial and temporal coverage.

REFERENCES

ADLER R. F., YEH H. Y., PRASAD N., TAO W. K. and SIMPSON J., *Microwave Simulation of Tropical Rainfall System with Three-Dimensional Cloud Model, J. Appl. Meteor.*, **31** (1991) 924.

ARKIN P. A. and MEISNER B. N., *The relationship between large scale convective rainfall and cold cloud over the western hemisphere during 1982-1984, Mon. Weath. Rev.*, **115** (1987) 51.

BATTAN L. J., *Radar Observations of the Atmosphere* (The University of Chicago Press) 1973.

CHIU L. S., *Estimating Areal Rainfall From Rain Area. Tropical Rainfall Measurements*, edited by J. S. THEON and N. FUGONO (A. Deepak Publishing, Hampton, Virginia) 1988, pp. 361-367.

DALU G., CADEDDU M. P., PRABHAKARA C. and SHORT D. A., *On the validation of ranfall retrieval algorithms for satellite microwave data, Nuovo Cimento C*, **21** (1998) 115-118.

DONEAUD A. A., IONESCU-NISCOV S., PRIEGNITZ D. L. and SMITH P. L., *The Area Time Integral as an Indicator for Convective Rain Volume, J. Climate Appl. Metor.*, **23** (1984) 555-561.

EBERT E. E., *Algorithm Intercomparison Project (AIP): Results of Third Algorithm Intercomparison Project (AIP-3)*, coordinated by E. E. EBERT (Bureau of Meteorology Research Center, Melbourne, Australia) 1996.

EBERT E. E., MANTON M. J., ARKIN P. A., ALLAN R. J., HOLPIN G. E. and GRUBER A., *Results from the GPCP Algorithn Intercomparison Programme, Bull. Am. Meteor. Soc.*, **77** (1996) 2875-2887.

HEYMSFIELD G. M., CAYLOR I. J., SHEPHERD J. M., OLSON W. S., BIDWELL S. W., BONCYK W. C. and AMEEN S., *Structure of Florida thunderstorms using high altitude aircraft radiometer and radar observations, J. Appl. Meteor.*, **35** (1996) 1736-1762.

HOUZE R. A. and BETTS A. K., *Convection in GATE, Rev. Geophys. Space Phys.*, **41** (1981) 541-576.

JONES D. M. A. and SIMS A. L., *Climatology of Instantaneous Rainfall Rates, J. Appl. Meteor.*, **17** (1978) 1135-1140.

KUMMEROW C., MACK R. A. and HAKKARINEN I. M., *A Self-consistency Approach to Improved Microwave Rainfall Estimation from Space, J. Appl. Meteor.*, **28** (1989) 869-884.

LOPEZ R. E., ATLAS D., ROSENFELD D., THOMAS J. L., BLANCHARD D. O. and HOLLE R. L., *Estimation of Rainfall Using the Radar Echo Area Time Integral, J. Appl. Meteor.*, **28** (1989) 1162-1175.

MCGHAUGHEY G. and ZIPSER E., *Passive microwave observations of the stratiform regions of two tropical oceanic Mesoscale Convective Systems, J. Appl. Meteor.*, **35** (1996) 1949.

MENEGHINI R. and KUMAGAI H., *Characteristics of the vertical profiles of dual-frequency, dual-polarisation radar data in stratiform rain, J. Atmos. Oceanic Technol.*, **11** (1994) 701-711.

OLSON W. S., KUMMEROW C., HEYMSFIELD G. M. and GIGLIO L., *A method for combined passive-active microwave retrievals of cloud and precipitation profiles, J. Appl. Meteor.*, **35** (1996) 1763-1789.

PETTY G. W. and KATSAROS K. B., *Nimbus 7 SMMR precipitation observations calibrated against surface radar during TAMEX, J. Appl. Meteor.*, **31** (1992) 489-505.

PRABHAKARA C., DALU G., LIBERTI G. L., NUCCIARONE J. J. and SUHASINI R., *Rainfall over Oceans: Remote Sensing from Satellite Microwave Radiometers, Meteor. Atmos. Phys.*, **47** (1992) 177-199.

SIMPSON J., *Tropical Rainfall Measurement Mission (TRMM): Report of the Science Steering Group* (NASA/GSFC, Greenbelt, MD), 1988.

SIMPSON J., KUMMEROW C., TAO W.-K. and ADLER R. F., *On the tropical rainfall measuring mission (TRMM), Meteor. Atmos. Phys.*, **60** (1996) 19-36.

SHORT D. A., KUCERA P. A., FERRIER B. S., GERLACH J. C., RUTLEDGE S. A. and THIELE O. W., *Shipboard Radar Rainfall Patterns within the TOGA/COARE IFA, Bull. Am. Meteor. Soc.* (1997) (in press).

SPENCER R. W., *A satellite passive 37 GHz scattering based method for measuring oceanic rain rates, J. Climate Appl. Meteor.*, **25** (1986) 754-766.

SMITH E. A. and MUGNAI A., *Foundations for Statistical-Physical Precipitation Retrieval from Passive Microwave Satellite Measurements. Part 1: Brightness Temperature Properties of a Time-Dependent Cloud Radiation Model, J. Appl. Meteor.*, **31** (1992) 532-552.

TAKAHASHI T., SUZUKI K., ORITA M., TOKUNO M. and DE LA MAR R., *Videosonde observations of precipitation processes in equatorial cloud clusters, J. Meteor. Soc. Jpn.*, **73** (1995), 509-534.

WILHEIT T. T., CHANG A. T. C. and CHIU L. S., *Retrieval of Monthly Rainfall Indices from Microwave Radiometric Measurements Using Probability Distribution Functions, J. Atmos. Oceanic Tech.*, 8 (1991) 118-136.

WU R. and WEINMAN J. A., *Microwave Radiances From Precipitating Clouds Containing Aspherical Ice, Combined Phase, and Liquid Hydrometeors, J. Geophys. Res.*, **89** (1984) 7170-7178.